Minivalley and Layer Control of Intermediate Twist Angle Double Bilayer Graphene

Chun Sum Brian Pang
Department of Physics and Astronomy, University of British Columbia, Vancouver, B.C., V6T 1Z1, Canada
(Dated: December 19, 2021)

In 2004, A. Geim and K. Novoselov successfully isolated monolayer graphene via mechanical exfoliation of graphite, marking a milestone in the field of condensed matter physics. Since then, immense effort has been devoted to investigate the novel phenomena in graphene and graphene-related structures, such as superconductivity in magic-angle twisted bilayer graphene. In this report, we will focus on the intriguing transport properties of twisted double bilayer graphene. In the first part, we will introduce preliminary concepts and terminologies for transport-related effects. Then, we will review the bandstructure of monolayer graphene and bilayer graphene to provide motivations for studying twisted double bilayer graphene in a multi-gated setup. In the last part, we will closely follow the work by de Vries *et al.*, in which they demonstrated the ability to fully control the minivalley and layer degrees of freedom of intermediate twist angle double bilayer graphene. It is expected that this report can deliver a succinct qualitative introduction to transport measurements, and demonstrate the potential of twisted double bilayer graphene in future electronics.

1. PRELIMINARIES

1.1. Hall Effect

When we pass a current through a two-dimensional electron gas in a uniform perpendicular-to-plane magnetic field, the current is deflected to the side of the sample, which is known as the Hall effect. In a two-dimensional Hall bar geometry, we can measure the longitudinal resistivity ρ_{xx} along the Hall bar, i.e. parallel to the unperturbed current flow; or the transverse resistivity ρ_{xy} across the Hall bar, i.e. perpendicular to the unperturbed current flow. The resistivity matrix is hence given by

$$\rho = \begin{pmatrix} \rho_{xx} & \rho_{xy} \\ -\rho_{xy} & \rho_{xx} \end{pmatrix}, \tag{1}$$

and the conductivity matrix is the inverse of the resistivity matrix, $\sigma = \rho^{-1}$ [1]. As most transport measurements will be conducted in a Hall bar sample geometry, the Hall effect is the central element of transport-related phenomena.

Note that the 2D samples are usually gated at the top and bottom for manipulation purposes. If we change the potential of the gates, we can draw charge carriers from the electrodes into the sample, or vice versa, thus tuning the Fermi level of the system.

1.2. Landau Level Broadening

It is well-known that when a two-dimensional electron gas is placed in a uniform perpendicular-to-plane magnetic field, the Hamiltonian can be rewritten in an analogous form to a simple harmonic oscillator, and the energy spectrum is discretized into Landau levels. If we consider Zeeman splitting of spins at the same time, we can get

$$E_n^{\pm} = \hbar\omega_c \left(n + \frac{1}{2}\right) \pm \frac{1}{2} g^* \mu_B B_z, \tag{2}$$

where $\omega_c = |e|B/m^*$ is the cyclotron frequency, g^* is the effective g-factor of electrons, and μ_B is the Bohr magneton [1]. Notice that the larger the magnetic field is, the larger the Landau level splitting is. If we plot the density of states against the energy, we should get a sum of Dirac delta functions:

$$\mathcal{D}_0(E, B) \propto \sum_{n,\sigma=\pm} \delta(E - E_n^{(\sigma)}). \tag{3}$$

However, no materials are perfect in reality. The presence of impurities or unevenly distributed charged dopants introduces scattering to the Landau electrons, causing them to possess a finite lifetime τ_q. This causes the density of states to broaden into a sum of Lorentzian distributions:

$$\mathcal{D}(E, B) \propto 2 \sum_n L_n \left(E - \hbar\omega_c \left(n + \frac{1}{2}\right)\right), \tag{4}$$

where $L_n(x_n)$ is the Lorentzian function centered at x_n with a full-width-half-maximum (FWHM) of $\hbar/\tau_q$ [1]. Note that in Eq. 4, we are working in a tricky limit of the magnetic field: we assumed the magnetic field to be small enough, such that many Landau levels are occupied at the ground state, i.e. Fermi level $E_F \gg \hbar\omega_c$, and the Zeeman splitting is too small to be resolved; but at the same time, we assumed the magnetic field to be large enough, such that the Landau level splitting is wider than the Lorentzian broadening [1]. After mathematical complications, the resulting density of states are shown in Fig. 1. We can see that the summed Lorentzian curves at finite magnetic field makes the density of states oscillatory. This provides a hint to understanding the Shubnikov-de Haas effect.

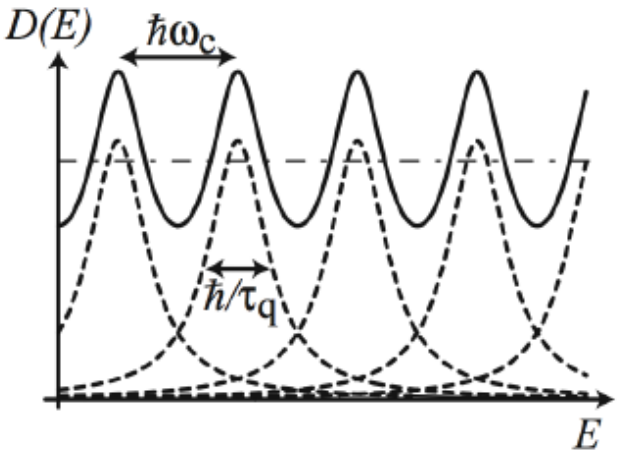

FIG. 1. Density of states of a practical 2D electron gas as a function of energy at finite magnetic fields (solid line) and zero magnetic fields (dashed line). Figure obtained from [1].

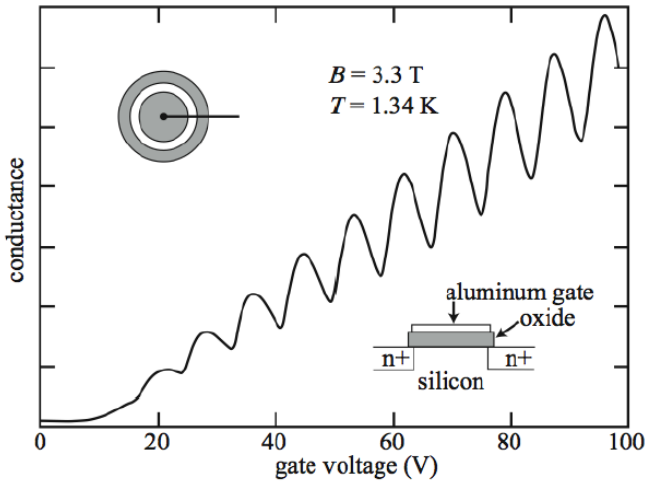

FIG. 2. SdH oscillation in longitudinal conductance for silicon surface, measured in a magnetic field of 3.3T and at a temperature of 1.34K. Figure obtained from [1] and reproduced from [3].

1.3. Shubnikov-de Haas effect

The Shubnikov-de Haas (SdH) effect refers to the oscillatory magneto-resistance in a 2D electron gas. When a perpendicular-to-plane magnetic field is applied to the sample in a gated Hall bar geometry, the longitudinal conductance σ_{xx} oscillates and increases as a function of the voltage applied at the top gate, as shown in Fig. 2. The complete descriptive formula of the SdH effect, also known as Ando formula, can be derived from Eq. 4 after intricate calculations (which will be omitted here) [1, 2]. Qualitatively, one can understand that the oscillating conductance in SdH effect originates from the oscillatory density of states after finite Landau level broadening. Since the SdH oscillation depends on the effective mass m^* of mobile charge carriers (electrons/holes) in the sample, experimentalists frequently determine the effective mass with this method [1]. This fact will help us with understanding the subsequently shown results of transportation measurements in twisted double bilayer graphene (TDBG).

2. ENERGY SPECTRUM OF MONOLAYER GRAPHENE AND BILAYER GRAPHENE

2.1. Monolayer Graphene

For monolayer graphene, we know that there are two inequivalent corners (also known as valleys) at the first Brillouin zone, namely K and K'. For a small crystal momentum $\vec{q}$ near the K (or K') point, we can write the Hamiltonian as [4]:

$$H(\vec{K}+\vec{q}) = \begin{pmatrix} 0 & \gamma_0\pi^\dagger \\ \gamma_0\pi & 0 \end{pmatrix}, \tag{5}$$

where γ_0 is the nearest neighbour hopping parameter, and $\pi = q_x + iq_y$. The fact that it is a 2×2 matrix comes from the two distinct Bloch states of different valleys. Since the above Hamiltonian is very similar to a Zeeman Hamiltonian, we will sometimes call the basis as "pseudospins" [4]. Calculating the energy spectrum, we can easily get linear dispersion (also know as Dirac cones) near the K and K' points.

To proceed, we need a brief introduction to the charge neutrality point (CNP). The CNP is defined as some specific energy level in the band structure, such that when the Fermi level resides at the CNP, the entire system becomes charge neutral [5]. For monolayer graphene, the CNP is at the tip of the Dirac cone, i.e. the Dirac point, at which the system is gapless. For insulators, the CNP is at the middle of the band gap. If a system has a wide band gap, the conduction band and valence band will be far from the CNP, causing the system to have a high peak resistance when the Fermi level is at the CNP [4].

2.2. Bilayer Graphene

By doubling the number of layers, bilayer graphene is more than doubly interesting as monolayer graphene. We assume a Bernal (AB) stacking of bilayer graphene as shown in Fig. 3. We define u as the interlayer potential difference, γ_1 as the nearest interlayer hopping, while γ_3 and γ_4 are the next-nearest neighbour interlayer hoppings. Then, approximating small γ_3 and γ_4,

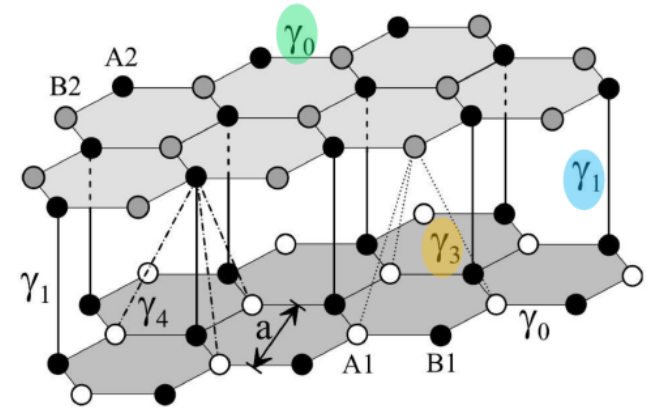

FIG. 3. Structure of bilayer graphene in Bernal stacking. γ_0 is the nearest neighbour hopping on the same layer. γ_1 is the nearest interlayer hopping. γ_3 and γ_4 are the next-nearest neighbour interlayer hoppings. Figure obtained from [6].

the Hamiltonian near K-point is [4]

$$H_K = \begin{pmatrix} u/2 & \gamma_0\pi^\dagger & 0 & 0 \\ \gamma_0\pi & u/2 & \gamma_1 & 0 \\ 0 & \gamma_1 & -u/2 & \gamma_0\pi^\dagger \\ 0 & 0 & \gamma_0\pi & -u/2 \end{pmatrix}. \tag{6}$$

By solving the Hamiltonian, we get the results as shown in Fig. 4. The spectrum now depends on the displacement field u, hence controllable by gating across the layers. At finite $u > 0$, the band gap opens and widens with increasing u. In Fig. 5, the (relatively small) variation of top-gate voltage V_{tg} for each curve corresponds to varying the Fermi level across the energy spectrum, while the (relatively large) change of bottom-gate voltage V_{bg} corresponds to significantly changing the band gap width. For a larger difference in top-gate and bottom-gate voltages, the band gap becomes larger, such that the CNP becomes further from the valence and conduction bands, leading to a higher peak resistance [7]. This is why for bilayer graphene, we need a top gate and a bottom gate to control the carrier density and displacement field separately.

Nevertheless, we are not satisfied yet. We would like a system that allows us to extract electronic states occupying different valleys upon request, such that we can exploit the pseudospin degree of freedom and make quantum devices. Again, it is time to stack up our system again – but with a little twist.

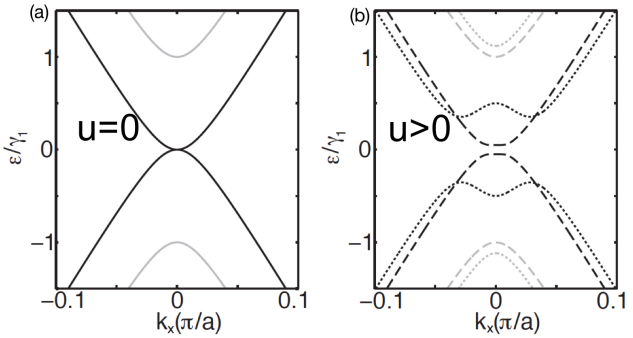

FIG. 4. (a) Energy spectrum around K point along k_x when $u = 0$. (b) Energy spectrum around K point along k_x when $u > 0$. Dashed (dotted) line represents the calculation without (with) γ_3 and γ_4. We shall only consider the dashed line in our discussion to avoid complication. Figure obtained from [1].

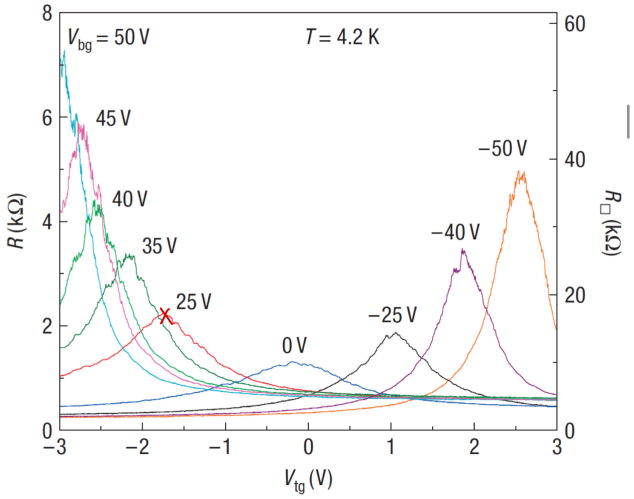

FIG. 5. Resistance against top-gate voltage V_{tg} for different values of bottom-gate voltage V_{bg} in a bilayer graphene sample. Figure obtained from [7].

3. TRANSPORT MEASUREMENTS OF INTERMEDIATE TWIST ANGLE DOUBLE BILAYER GRAPHENE

This section will closely follow the discovery of de Vries *et al.* in 2020 [8].

3.1. Moiré Superlattice and the Twist Angle

When two bilayers of graphene (four monolayers in total) are stacked together with a rotational mismatch, a twisted double bilayer graphene (TDBG) is obtained. The lattice mismatch gives rise to a large-scale interference pattern known as the moiré pattern. As the system respects a discrete translational symmetry of the moiré

pattern, a moiré superlattice is effectively introduced to the system, with an enlarged unit cell in real space. Hence, in the reciprocal space, the system will possess a mini-Brillouin zone (mini-BZ) as shown in Fig. 6 [8].

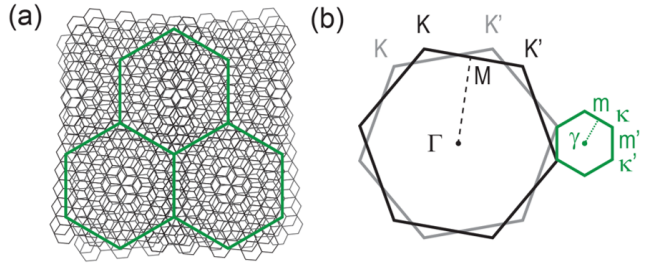

FIG. 6. (a) Moiré pattern of TDBG in real space. The Moiré unit cell is marked in green. (b) Mini-BZ constructed from the BZ of individual bilayers. Figure obtained from [8].

At small twist angles ($< 1°$), the two layers in TBG or TDBG becomes highly coupled [9]. Near the magic angle ($\sim 1°$), the spectrum possesses flat bands and strongly correlated states dominate the behaviour, leading to insulating or superconducting phases [10, 11]. At large twist angles ($> 10°$), the two layers becomes decoupled, that states from individual layers do not interact and can be tuned separately [12]. However, the behaviour of TDBG at intermediate twist angles ($\sim 2°$) remained a mystery, thus motivating de Vries *et al.* to investigate the limit. Using the tear-and-stack method [13], they fabricated a TDBG sample with a twist angle of 2.37°, and with top and bottom gates [8].

3.2. Theoretical Calculation at Zero Displacement Field

The group first calculated the energy spectrum and the wavefunction probability distribution of the TBDG as shown in Fig. 7 [8]. From Fig. 7(a), we can first see that the energy spectrum has interesting Fermiology. If the Fermi level is at the lower region of the conduction band, it is populated by κ and κ' states at the mini-BZ corners with a positive band curvature, i.e. electron-like behaviour. However, if the Fermi level is at the higher region of the conduction band, it is dominated by γ states at the mini-BZ center with a negative band curvature, i.e. hole-like behaviour [8]. Such a change between the two contrasting behaviours of carriers is called a Lifshitz transition [4]. Then, from Fig. 7(b), we notice that the γ states are widespread throughout the four layers, but the κ and κ' states are relatively localized in separate bilayers. The minivalley degree of freedom is coupled to the layer degree of freedom. This implies if we can make the states only occupy the κ sites but not the κ' sites, we can control the mobile states to be mainly localized at the upper bilayer [8]. In other words, we can make only one layer conducting, and another layer insulating by gapping out the states there.

3.3. Experimental Results

By applying a perpendicular-to-plane magnetic field and varying the top and bottom gates potential, de Vries *et al.* measured the conductance G of the sample[8]. They plotted the numerical derivative of conductance as a function of top-gate and bottom-gate voltages in Fig. 8(a). For the phase diagram in Fig. 8(b), they used the capacitor model for calculation: with C_{tg} and C_{bg} as the capacitance of top-gate-TDBG interface and bottom-gate-TDBG interface respectively, they set the total carrier density $n \propto C_{bg}V_{bg} + C_{tg}V_{tg}$, and the displacement field $D \propto C_{bg}V_{bg} - C_{tg}V_{tg}$ [8]. They further calculated the band structures of the system in zero displacement field (Fig. 8(c)) and non-zero displacement field (Fig. 8(d)) [8].

First of all, the fringe-like pattern in Fig. 8(a) is exactly the long-awaited SdH effect, as one can compare with Fig. 2. Immediately, we can identify type 1 regions as those with crossed stripes, implying there are two sets of SdH oscillations with different coupling strengths to the top-gate and the bottom-gate. If we compare with Fig. 8(c), we know that type 1 regions are just the phase containing two decoupled carrier gases at κ and κ', i.e. at the upper and lower bilayers [8]. For the κ states in the upper bilayer, the effect of V_{bg} is screened by the κ' states, so the κ states are more strongly affected by V_{tg} [8]. Similarly, the κ' states in the lower bilayer are more strongly affected by V_{bg}. This accounts for the different slopes of SdH pattern of the two gases.

As we move the Fermi level past the van-Hove singularity in Fig. 8(c), the system undergoes a Lifshitz transition and becomes dominated by γ states. Since γ states spread across all layers (as seen in Fig. 7(b)) and does not distinguish between minivalleys, we can say that the γ states form a collective, coupled carrier gas [8]. This corresponds to type 2 regions in Fig. 8(a), with only one set of SdH pattern.

The truly fascinating part only exists for non-zero displacement field D, labelled as type 3 regions in Fig. 8(a). Again, from the uniform SdH stripes, we can infer that there is only one type of carrier gas in type 3 regions. However, when comparing to Fig. 8(d), due to the minivalley asymmetry of the band structure, each type 3 region only contains one decoupled κ (or κ') gas, with the other species gapped out [8]. This means the states in type 3 regions are mainly localized in the uppermost (or lowermost) layer. Therefore, by tuning the displacement

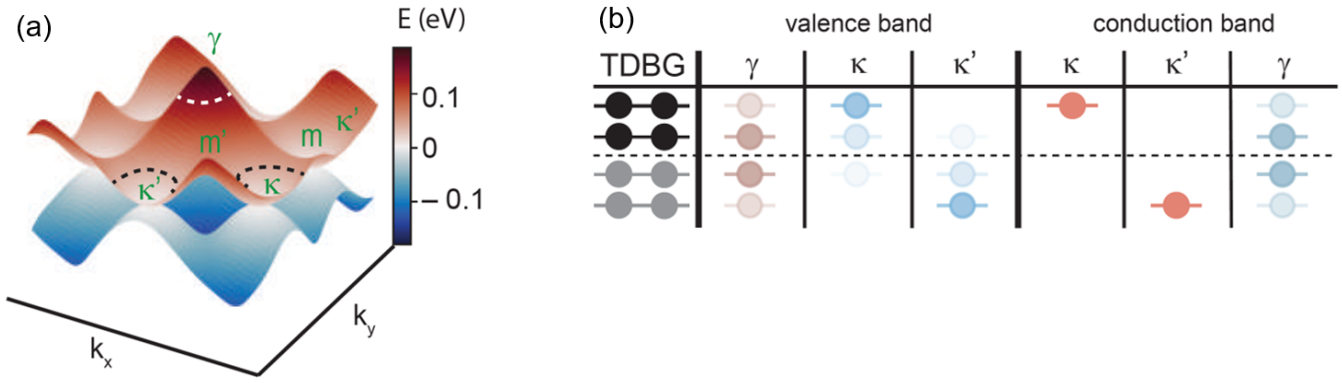

FIG. 7. (a) Calculated energy spectrum of the TBDG system with respect to the mini-BZ at zero displacement field. (b) Calculated wavefunction probability distributions at different layers at zero displacement field. Red colour stands for electrons and blue colour stands for holes. Darker colour means a higher probability density. Figure obtained from [8].

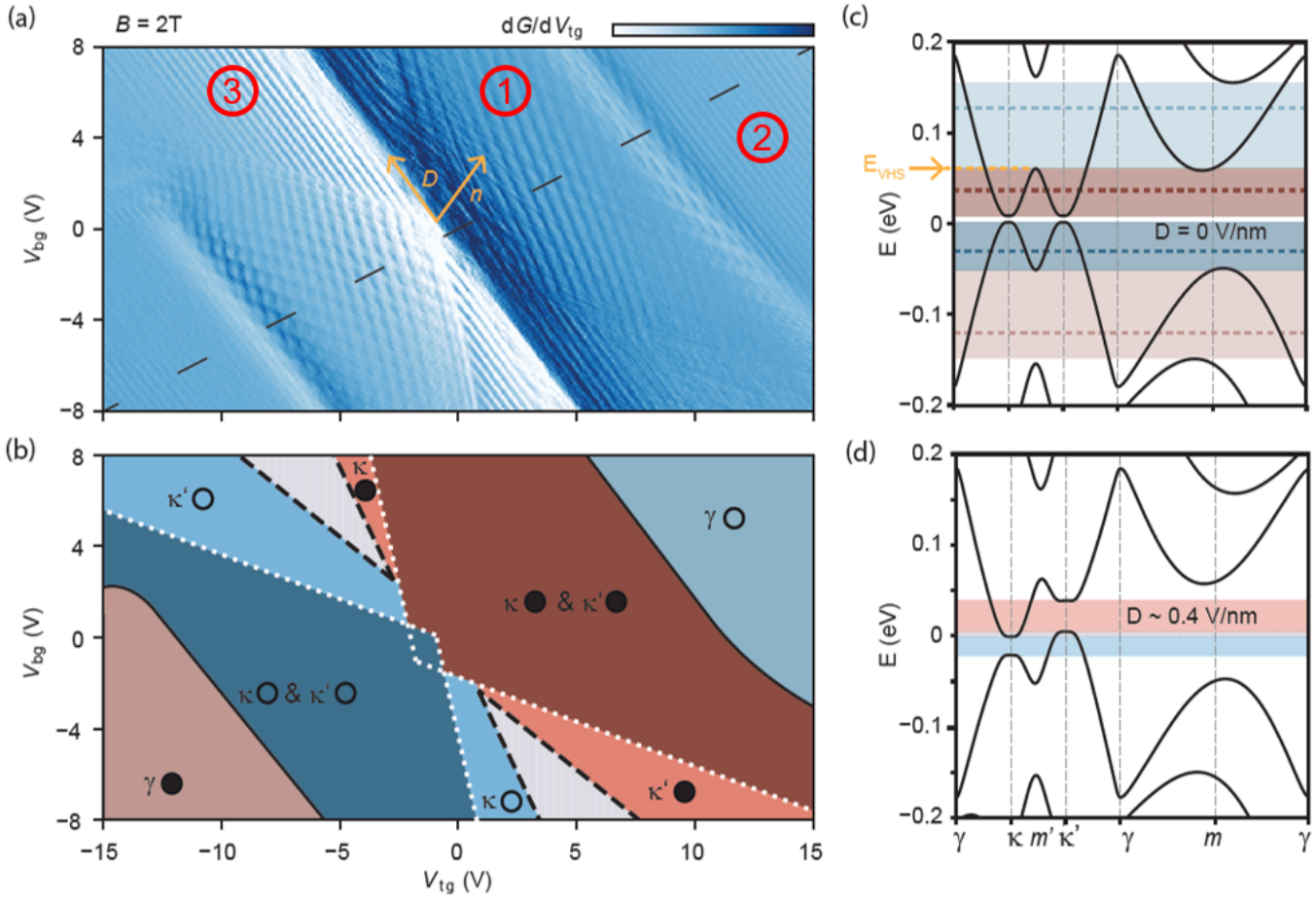

FIG. 8. (a) Plot of the numerical derivative of measured conductance G as a function of the top-gate voltage V_{tg} and bottom-gate voltage V_{bg} at $B = 2T$. The axis of increasing carrier density n and increasing displacement field D are shown. The graph is divided into three types of region for analysis. (b) Theoretical calculation of phase diagram of the system. Red colour stands for electrons and blue colour stands for holes. (c,d) Energy spectrum calculations at displacement fields $D = 0V/nm$ and D $0.4V/nm$. The shaded colours correspond to those in (b). The energy for van Hove singularity E_{VHS} is marked in orange. Figure obtained from [8].

field using V_{tg} and V_{bg}, the minivalley (and hence the layer) of the carrier gas can be freely chosen [8]. The group has successfully realized a complete minivalley and layer polarization in TDBG. By treating the minivalley degree of freedom as pseudospins, it is promising to utilize TDBG in future valleytronic devices, where the "pseudo-spin-up" and "pseudo-spin-down" states can be used as qubit basis states [14]. The diverse landscape of phases in TBDG is also attractive for further investigation and manipulation.

4. CONCLUSION

Throughout this report, we qualitatively reviewed some basic concepts in electronic transport of 2D materials, including Hall effect, Landau level broadening, and Shubnikov-de Haas effect, in order to aid our comprehension of the transport phenomena in twisted double bilayer graphene. We also reviewed the energy spectrum of monolayer and bilayer graphene to understand the motivation to investigate TBDG systems. Finally, we appreciated how de Vries *et al.* successfully achieved a full minivalley and layer control of states in TBDG, proving the potential of the material to be employed in next-generation quantum devices. With relentless efforts, scientists will continue to discover and fabricate more fascinating materials, perhaps just with a slight twist.

REFERENCES

[1] Ihn, T. (2009). Semiconductor Nanostructures: Quantum states and electronic transport. OUP Oxford.

[2] Ando, T., Fowler, A. B., & Stern, F. (1982). Electronic properties of two-dimensional systems. Reviews of Modern Physics, 54(2), 437.

[3] Fowler, A. B., Fang, F. F., Howard, W. E., & Stiles, P. J. (1966). Magneto-oscillatory conductance in silicon surfaces. Physical Review Letters, 16(20), 901.

[4] Ihn, T. (2020, April). Graphene. Electronic Transport in Nanostructures. ETH Zürich.

[5] Tung, R. T. (2014). The physics and chemistry of the Schottky barrier height. Applied Physics Reviews, 1(1), 011304.

[6] McCann, E., & Koshino, M. (2013). The electronic properties of bilayer graphene. Reports on Progress in physics, 76(5), 056503.

[7] Oostinga, J. B., Heersche, H. B., Liu, X., Morpurgo, A. F., & Vandersypen, L. M. (2008). Gate-induced insulating state in bilayer graphene devices. Nature materials, 7(2), 151-157.

[8] de Vries, F. K., Zhu, J., Portoles, E., Zheng, G., Masseroni, M., Kurzmann, A., ... & Rickhaus, P. (2020). Combined minivalley and layer control in twisted double bilayer graphene. Physical Review Letters, 125(17), 176801.

[9] San-Jose, P., & Prada, E. (2013). Helical networks in twisted bilayer graphene under interlayer bias. Physical Review B, 88(12), 121408.

[10] Cao, Y., Fatemi, V., Demir, A., Fang, S., Tomarken, S. L., Luo, J. Y., ... & Jarillo-Herrero, P. (2018). Correlated insulator behaviour at half-filling in magic-angle graphene superlattices. Nature, 556(7699), 80-84.

[11] Cao, Y., Fatemi, V., Fang, S., Watanabe, K., Taniguchi, T., Kaxiras, E., & Jarillo-Herrero, P. (2018). Magic-angle graphene superlattices: a new platform for unconventional superconductivity. arXiv preprint arXiv:1803.02342.

[12] Rickhaus, P., Zheng, G., Lado, J. L., Lee, Y., Kurzmann, A., Eich, M., ... & Ensslin, K. (2019). Gap opening in twisted double bilayer graphene by crystal fields. Nano letters, 19(12), 8821-8828.

[13] Kim, K., Yankowitz, M., Fallahazad, B., Kang, S., Movva, H. C., Huang, S., ... & Tutuc, E. (2016). van der Waals heterostructures with high accuracy rotational alignment. Nano letters, 16(3), 1989-1995.

[14] Vitale, S. A., Nezich, D., Varghese, J. O., Kim, P., Gedik, N., Jarillo-Herrero, P., ... & Rothschild, M. (2018). Valleytronics: opportunities, challenges, and paths forward. Small, 14(38), 1801483.